Journal of Applied Polymer Science

Effective Thermal Conductivity of 3,5-Diaminobenzoyl-Functionalized Multiwalled Carbon Nanotubes/Epoxy Composites

Uraiwan Pongsa and Anongnat Somwangthanaroj
Department of Chemical Engineering, Faculty of Engineering, Chulalongkorn University, Bangkok 10330, Thailand
Correspondence to: A. Somwangthanaroj (E-mail: anongnat.s@chula.ac.th)

ABSTRACT: To obtain homogeneous dispersion and good interfacial interaction between MWCNT and polymer matrix, the functionalization of MWCNTs with 3,5-diaminobenzoic acid (DAB) via a direct Friedel-Crafts acylation was accomplished. FTIR, XPS, and FT-Raman analysis was performed to confirm that diaminobenzoyl moieties were successfully grafted onto MWCNT surface with less structural damage. The incorporation of diaminobenzoyl-functionalized MWCNTs (DAB-MWCNTs) into epoxy matrix can substantially enhance storage modulus (E') as well as glass transition temperature (T_g) and reduce the coefficient of thermal expansion. The thermal conductivity enhancement can be observed with DAB-MWCNTs probably due to good dispersion and decreased interfacial thermal resistance between MWCNT and polymer matrix. The Maxwell-Eucken, Lewis-Nielsen, and MG-EMA models were used to evaluate theoretical thermal conductivity. Moreover, epoxy resin incorporated with hybrid fillers, which consisted of DAB-MWCNTs and silicon nitride exhibit higher thermal conductivity than those with single filler, thereby forming perfectly heat conductive pathways. © 2013 Wiley Periodicals, Inc. J. Appl. Polym. Sci. 130: 3184–3196, 2013

KEYWORDS: composites; nanotubes; graphene and fullerenes; spectroscopy; surfaces and interfaces; theory and modeling

Received 6 February 2013; accepted 8 May 2013; Published online 14 June 2013
DOI: 10.1002/app.39520

INTRODUCTION

In past few years, smart devices with ultrathin, light weight, and multifunction have become very popular. The increasing interest in these devices has heightened the need for advanced microelectronic packaging appropriate to use in electronics. As continuous development in the miniaturization, the heat dissipation is still a critical problem in packaging, limiting the reliability, and high performance. Therefore, the polymer-based composite with high thermal conductivity has been received more attention. Traditionally, polymer composite with high thermal conductivity can be obtained by incorporation of inorganic particles with intrinsically high thermal conductivity, providing heat conductive networks in the composite.[1–3] The formation of effective heat conductive pathways is promoted by an increase of thermally conductive filler loading, commonly higher than 30 vol %, thereby enhancing the heat dissipation ability.[4,5] However, the introduction of high filler concentration into polymer matrix results in an increase of viscosity and limitation of processability.

One solution to this problem might be using the filler with large aspect ratio at lower content to maximize the randomly heat conductive networks in the composites. Multiwalled carbon nanotubes (MWCNTs) are one of the most attractive filler candidates because of their outstanding characteristic including nanostructure, high aspect ratio, excellent mechanical, and thermal properties. Especially, MWCNTs show exceptionally high thermal conductivity, thus MWCNTs is often used in the thermal management applications. It is known that the advantage of MWCNTs certainly depends on the degree of dispersion. MWCNTs easily form large agglomerates and are hardly dispersed in polymer matrix due to their high surface area and intrinsic van der Waals force. Besides, weak interfacial interaction between MWCNT and polymer matrix results in a lack of load transfer and heat transfer in polymer composite. These behaviors hinder potential of using MWCNTs to obtain targeted properties. Accordingly, an approach to achieve individual tube dispersion and good interfacial interaction of MWCNTs is a challenge. The surface modification has widely been considered to overcome the limitation in MWCNT manipulation. MWCNTs were often treated by the harsh chemical oxidation in strong acids to generate the carboxylic and oxygen-containing groups on their surfaces to facilitate further functionalization or fabrication.[6,7] Although, better dispersion and interfacial interaction can be achieved via this method, the dramatic structural damages on the surface of MWCNTs can easily occur. Consequently, much attention has been focused on the alternative functionalization methods without or less structural damage. Among various methods of surface modification, it was found that a direct Friedel-Crafts acylation, the functionalization

© 2013 Wiley Periodicals, Inc.

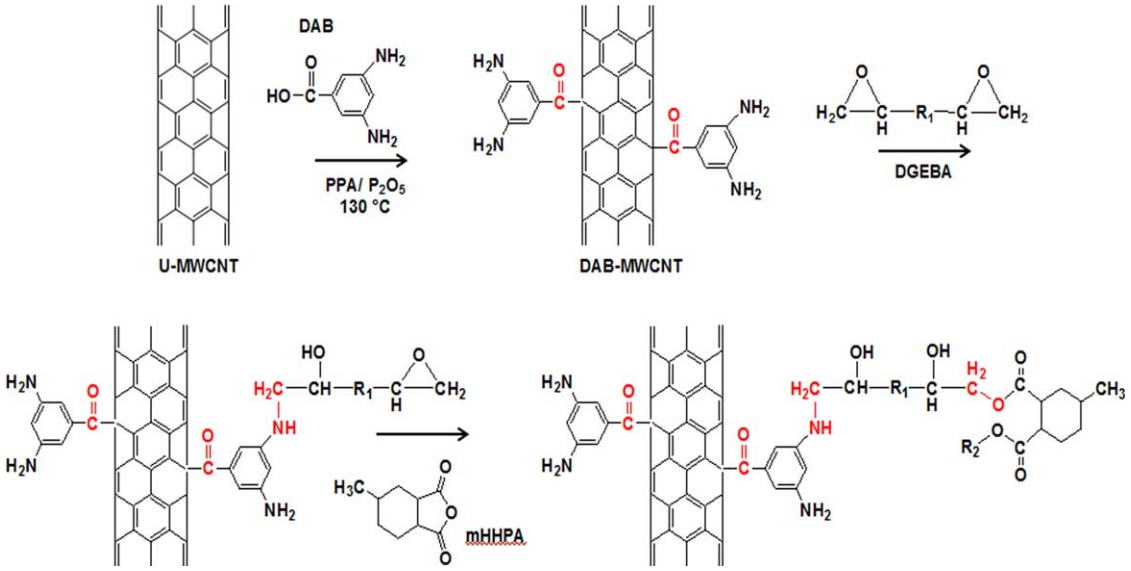

Figure 1. Procedure of diaminobenzoyl-functionalized MWCNT/epoxy composite. [Color figure can be viewed in the online issue, which is available at wileyonlinelibrary.com.]

reaction, is convenient and effective for the purification and the functionalization of the reactive functional groups onto MWCNT surface in a one-pot process with trace amounts of defects. [8–10]

Furthermore, the crucial objective of this work is to improve the thermal conductivity of epoxy resin for using in microelectronic packaging, which requires insulation properties. Therefore, the content of electrically conducting MWCNTs should be kept as low as possible but still high enough for good heat dissipation. Many recent studies have focused on the addition of hybrid filler systems into the polymer matrix. Polymer composites containing MWCNTs and thermally conductive particles such as boron nitride,[11] aluminum nitride,[12] and silicon carbide[13,14] have been conducted. Because partial replacement of micron-sized inorganic filler into the space formed in MWCNT-to-MWCNT networks can be obtained more heat, conductive pathways with high packing density that facilitate phonon transfer leading to high thermal conductivity. Among commonly used inorganic particles, Silicon nitride (Si_3N_4) is one of attractive inorganic fillers because of its high thermal conductivity as well as low coefficient of thermal expansion (CTE) and more commercially available than boron nitride.[15–18] However, there has not been the study of effects of Si_3N_4 particles mixed with MWCNTs as hybrid fillers on the thermal conductivity and dynamic mechanical properties yet. Particle size of fillers is one of the most important factors for the enhancement of thermal conductivity. The micron-sized fillers effectively achieve the thermal conductivity of composites, but the settling of fillers in polymer matrix is often observed. In case of nano-sized fillers, the thermal conductivity of composites exceptionally increases with low filler loading. Due to high surface area of nano-sized particles, the strong agglomeration occurred and thus the surface modification and effective mixing method are required to improve the dispersion, thereby increasing the production costs. Besides, the viscosity of composites intensely increases that hinders the processability. To avoid agglomeration of filler and to obtain low viscous epoxy resin for ease in industrial processing, the submicron-sized Si_3N_4 is considered as ideal filler to generate the hybrid filler with perfect thermal conductive networks.

Consequently, this study was designed to evaluate the effect of surface functionalization with a reactive reactant, that is, 3,5-diaminobenzoic acid (DAB) via Friedel-Crafts acylation in a one-pot process on the surface properties of MWCNTs. The diaminobenzoyl (DAB) compound was effectively introduced onto the MWCNT surface with less structural damage as confirmed by FTIR, XPS, and FT-Raman results. The amino functional groups on the surface of DAB-MWCNTs provided the good dispersion and chemical interaction with epoxy matrix, resulting in the decrease of interfacial thermal resistance, and thus the thermal conductivity of composites increased. Moreover, the hybrid filler systems between unmodified MWCNTs (U-MWCNT) or diaminobenzoyl-functionalized MWCNTs (DAB-MWCNT) and submicron-sized Si_3N_4 particles were conducted in this work. In this system, the MWCNT networks serve as the skeleton and Si_3N_4 particles facilitate the thermal transport along the MWCNT networks, thus providing high packing density and enhancing the overall thermal properties of the materials. The theoretical thermal conductivities were also determined by using the Maxwell-Eucken, Lewis-Nielsen, and MG-EMA models. Moreover, the dynamic mechanical and thermal properties of composites were investigated.

EXPERIMENTAL

Materials

Diglycidyl ether of bisphenol A (DER331, MW 372) from Dow Chemical Company, hexahydro-4-methylphthalic anhydride (96%) and cobalt (II) acetylacetonate (CoIIAcAc) from Sigma-Aldrich were used as polymer matrix, curing agent, and catalyst, respectively. Multiwalled carbon nanotubes (MWCNTs)

purchased from Chengdu Organic Chemicals Company (Chinese Academy of Sciences) and submicron-sized Si_3N_4 (1 μm) from Sigma-Aldrich Co were used as filler. MWCNTs were synthesized by a chemical vapor deposition process and have a dimension of 8 nm OD and 10 μm length. Polyphosphoric acid (PPA, 83% assay) and phosphorus pentoxide (P_2O_5) from Sigma-Aldrich were used as a reaction medium for the functionalization in which DAB from Sigma-Aldrich was used as functionalizing reactant.

Preparation of DAB-Functionalized MWCNTs

In this work, MWCNTs were covalently functionalized with DAB moieties via electrophilic substitution reaction, which was called a direct Friedel-Crafts acylation in a mild PPA/P_2O_5 medium. Due to its moderate acidic, PPA not only promoted the oxidation of metallic impurities and carbonaceous fragments on the surface of MWCNTs, but also effectively catalyzed the Friedel-Crafts reaction. Besides, the viscous characteristic of PPA could impede the reaggregation of MWCNTs. P_2O_5 was used as a dehydrating agent to promote the functionalization. The scheme of reaction is demonstrated in Figure 1 and the experimental details are described as follows. The specific weight of DAB, as-received MWCNTs, PPA, and P_2O_5 were placed in a 100 mL round-bottom flask equipped with a mechanical stirrer, nitrogen inlet, and outlet. This mixture was stirred at 130°C for 72 h under dry nitrogen purge. Distilled water was added to the mixture after cooling down to room temperature. The obtained MWCNTs separated by centrifuge were stirred in acetone for 1 day to remove unreacted chemicals. The MWCNT solution was then separated by centrifuge. The above-mentioned purification steps were repeated for 2–3 times. After that, the MWCNTs were washed with distilled water and separated by centrifuge. Then, the collected powder was freeze dried for 3 days to remove remaining solvent. In this research, unmodified MWCNTs and 3,5- DAB-functionalized MWCNTs are defined as U-MWCNT and DAB-MWCNT, respectively.

Preparation of Epoxy Composites

Owing to poor dispersion of MWCNTs in epoxy, U-MWCNTs or DAB-MWCNTs were firstly sonicated in the curing agent that was also acted as a solvent due to its low viscosity for 30 min. In case of hybrid filler systems, submicron-sized Si_3N_4 particles were mixed and sonicated in MWCNT mixture. Epoxy was then added and stirred in the mixture. The catalyst was dissolved in the mixture by ultrasonication for 30 min. The mixture was then stirred until homogeneous. The obtained mixture was transferred to aluminum mold and degassed in a vacuum oven. After curing at 230°C for 1 h, the sample was slowly cooled down to room temperature. The mold was peeled off and the sample was polished for further analysis.

Characterization

Fourier Transform Infrared Spectrometry. To investigate the functional groups on MWCNT surface before and after the functionalization, FTIR spectra were conducted by using a Spectrum GX FTIR spectrometer (Perkin Elmer). The powder sample and KBr powder were ground together. The ground powder was pressed into pellet with a smooth surface. The pellet was loaded into a sample holder and then placed in a chamber. All FTIR spectra were collected in a range of 4000–650 cm^{-1} with a resolution of 4.0 cm^{-1} under continuous nitrogen flow.

X-ray Photoelectron Spectroscopy. Surface chemistry of U-MWCNTs and DAB-MWCNTs was evaluated by using XPS. XPS analysis was performed by using an AMICUS photoelectron spectrometer equipped with a Mg K_α X-ray as a primary excitation and a KRATOS VISION2 software. The XPS curve fitting of C1s, O1s, and N1s was accomplished by Origin 8.1.

Fourier Transform Raman Spectroscopy. The effect of functionalization on the structural quality of MWCNTs was examined by using a Spectrum GX FT-Raman spectrometer (PerkinElmer). FT-Raman analysis was performed over a range of 0–1000 cm^{-1} with a laser in the near infrared-usually at 1064 nm.

Thermogravimetric/Differential Thermal Analysis. The thermal stability of MWCNTs before and after the functionalization was evaluated by using a Diamond TG/DTA instrument (PerkinElmer). Samples were loaded in ceramic pans and then heated to 800°C at 10°C/min under nitrogen atmosphere at 100 mL/min flow rate.

Scanning Electron Microscopy. Morphology of the fracture surface of epoxy composites was observed by using a Hitachi S-3400 scanning electron microscope (SEM) to study the dispersion of fillers in the polymer matrix. All samples were quenched in liquid nitrogen and fractured to obtain the cross-sections. The samples were then sputter coated with gold before the SEM observation.

Dynamic Mechanical Analysis. The dynamic mechanical properties of epoxy composites were investigated by using a Pyris Diamond DMA instrument (Perkin-Elmer). The bending mode was performed at a frequency of 1 Hz for all of samples. The samples were heated from room temperature to 250°C at a heating rate of 5°C/min under N_2 atmosphere.

Thermomechanical Analysis. The CTE of all samples was determined by using a Pyris Diamond TMA instrument (Perkin-Elmer). The expansion probe was performed with 3 m*N* of static force. The temperature was scanned from room temperature to 250°C at a heating rate of 5°C/min under N_2 atmosphere.

Thermal Conductivity Analysis. The laser-flash thermal conductivity measurement was performed in this work. The measurement of thermal diffusivity was conducted by using a LFA 1000 Laser flash (NETZSCH, Germany). The sample surface was irradiated with very short laser pulse and temperature rise was measured on the opposite side of the sample, leading to calculating the thermal diffusivity. Specific heat capacity was measured by using a Pyris Diamond DSC instrument (PerkinElmer). In addition, the bulk density of the specimen was measured by water displacement.

RESULTS AND DISCUSSION

Functionalization of MWCNTs

To obtain great performance of MWCNTs as reinforcing filler in polymer composites, enhancing dispersion and interfacial interaction between MWCNT and polymer matrix is necessary. In

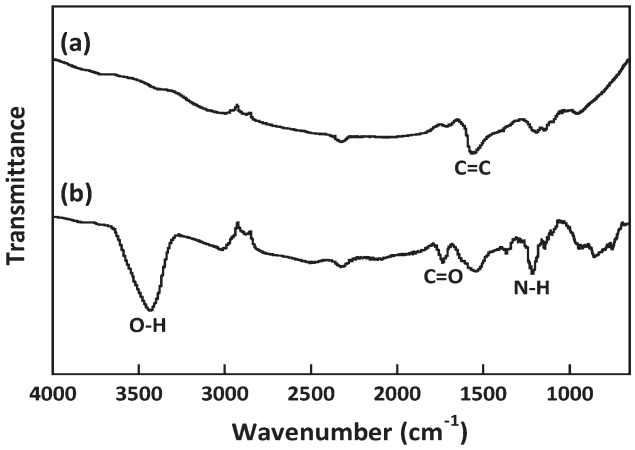

Figure 2. FTIR spectra of (a) U-MWCNTs and (b) DAB-MWCNTs.

this study, MWCNTs were directly functionalized with DAB moieties via Friedel-Crafts acylation. Surface of MWCNTs would be treated with DAB functional groups, which were helpful for further composite fabrication. Surface chemistry of MWCNTs before and after the functionalization was investigated by using FTIR as illustrated in Figure 2. It was clearly seen that U-MWCNTs show a peak at ~1567 cm^{-1} assigned to aromatic C═C stretch of benzene ring and a small peak at ~1189 cm^{-1} corresponded to C—O stretch of the phenols.[19,20] It revealed that there were small amounts of oxygen-containing groups established on the surface of U-MWCNTs. After the functionalization, DAB-MWCNTs exhibit peaks at ~1216, ~1736, and ~3435 cm^{-1}, which can be ascribed to N—H stretch of primary aromatic amine, C═O stretch of carbonyl group and N—H stretch of amine groups, respectively.[21,22] The presence of these peaks indicated that DAB functional group was successfully introduced onto the surface of MWCNTs through the carbonyl group.

Additionally, XPS analysis was conducted to determine the elements of MWCNTs before and after the functionalization. Figure 3 shows XPS survey spectra of the samples. Peaks of C1s at ~285 eV and O1s at ~534 eV can be attributed to the carbon structures of MWCNTs and oxygen-containing groups on MWCNT surfaces, respectively.[23] As expected, the N1s peak was only visible in the spectrum of DAB-MWCNTs at ~400.2 eV (N—C), indicating the existence of amino groups on their surface.[24,25] The surface element composition of U-MWCNTs and DAB-MWCNTs based on the ratios of peak areas from XPS analysis was summarized in Table I. Relative concentration of O and N atoms noticeably increased after the functionalization whereas the amounts of C atom significantly decreased. It is possibly due to the introduction of diaminobenzoyl (DAB) functional groups onto surface of MWCNTs. The fitting spectra of C1s and O1s were performed to acquire more informative bonding structure of MWCNTs before and after the functionalization. To identify the type of carbon bonding, the C1s peaks were deconvoluted into several Gaussian peaks, as depicted in Figure 4(a,b). The main peak at 284.2–284.5 eV represents the sp^2-hybridized graphite-like carbon atoms (C═C). The peak at around 285.2–285.5 eV corresponds to the sp^3-hybridized diamond-like carbon atoms (C—C), referring to the defects on the nanotube structure. Various carbon-oxygen functionalities on the MWCNT surface were observed as the following small peaks at 286.1–286.3 eV (C—O), 286.6 eV (C—NH_2), 287.4–287.6 eV (C═O), and 288.1 eV (COOH).[25] Also, the peak at 290.8 eV can be assigned to π-π^* transition. It was an interesting phenomenon that the relative concentration of C═C remarkably decreased while the concentration of C═O and C—NH_2 increased after the functionalization. It is due to the fact that some of C═C structures were possibly interrupted and altered to C—C structures because of the attachment of DAB moieties during the functionalization. These results are consistent with previous publications.[20,25] Besides, the deconvolution of the O1s spectra exhibit the two peaks assigned to O═C at 351.6–351.7 eV and O—C at 533.3–533.6 eV.[6,24,25] Figure 4(c,d) shows the deconvolution of O1s spectra of U-MWCNT and DAB-MWCNT, respectively. Relative concentration of O═C significant increased for the functionalized sample. It is possibly due to grafting of DAB moieties onto the MWCNT surface through reactive carboxyl groups.

Moreover, FT-Raman spectroscopy was performed to evaluate the effect of functionalization on the structural destruction of MWCNTs. FT-Raman spectra for unmodified and functionalized MWCNTs are shown in Figure 5. It is obviously shown that the two characteristic bands located at ~1590 and ~1284 cm^{-1} commonly refers to the in-plane tangential mode (G band) for the stretching vibrations of the sp^2-hybridized carbons (C═C) and the disorder-induced modes (D band) of the sp^3-hybridized carbons or defects (C—C), respectively. The ratio

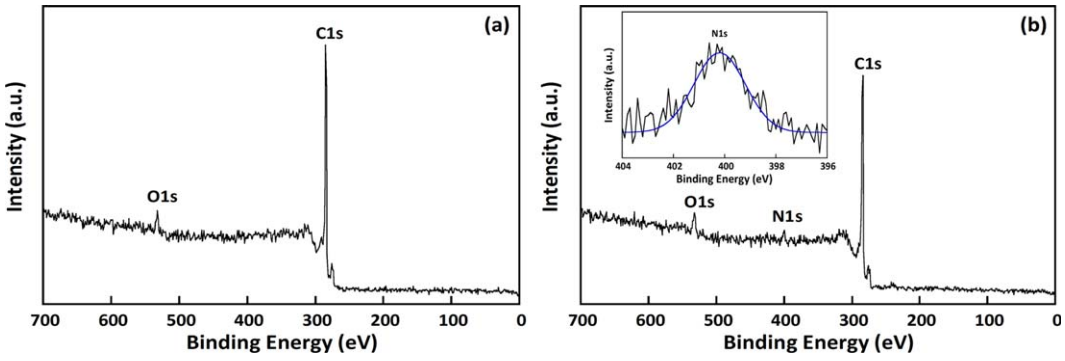

Figure 3. XPS survey spectra of (a) U-MWCNTs and (b) DAB-MWCNTs.

Table I. Surface Elements of MWCNTs Before and After the Functionalization

	Atomic concentration (%)					Grafting density (%)	
Material	C1s	O1s	N1s	O/C (%)	N/C (%)	XPS	TGA
U-MWCNT	90.20	9.80	-	0.11	-	-	-
DAB-MWCNT	79.82	15.83	4.35	0.20	0.05	2.18	2.21

of integral area of D band to G band (I_D/I_G) is often used to investigate the amount of defects in nanotube structure before and after the functionalization.[26] The FT-Raman results are summarized in Table II. It was found that the I_D/I_G ratio of DAB-MWCNTs (I_D/I_G = 0.455) was higher than that of U-MWCNTs (I_D/I_G = 0.449). This result revealed that the amount of the sp^3-hybridized carbons or defects on the MWCNT surface increased after the functionalization because some of C═C structures were interrupted possibly due to the grafting of DAB moieties and converted to C—C structures. However, the I_D/I_G ratio of MWCNTs functionalized with DAB via this method was not significantly changed, comparing with the conventional surface treatment. It is confirmed that functionalized MWCNTs were obtained with less structural damage. It is because MWCNTs were functionalized in the mild medium reaction, which could introduce DAB moieties onto the surface of MWCNTs via covalent bonds but it was not too strong to generate many defects on their surface.

Thermal Stability of MWCNTs

To evaluate thermal stability in N_2 atmosphere of MWCNTs before and after functionalization, TGA measurement was conducted from room temperature to 800°C. TGA thermograms of U-MWCNTs and DAB-MWCNTs are shown in Figure 6. U-MWCNTs show stable thermal behavior without significant weight loss at below 600°C, however; disordered and amorphous carbons on their surface were obviously decomposed at 650°C. In comparison, the weight of DAB-MWCNTs remarkably decreased in temperature range of 250 to 600°C because oxygen-containing groups and diaminobenzoyl moieties attached on their surface were stripped off. This phenomenon is similar to the TGA results reported in many researches involving the surface treatment of MWCNTs.[10,27] Finally, thermal degradation of remaining disordered carbons of DAB-MWCNTs was clearly observed at temperature higher than 600°C. From TGA results, the calculated grafting density of diaminobenzoyl moieties in DAB-MWCNTs is 2.21 mol %.

Dispersion of MWCNTs

Generally, properties of composites can be effectively enhanced by achieving a homogeneous dispersion of fillers and good interfacial interaction between polymer matrix and filler. Thus, the dispersion of MWCNTs in polymer matrix is also investigated in this work. The fracture surfaces of epoxy composites were observed by using SEM as displayed in Figure 7. The fracture surface of neat epoxy is relatively smooth which commonly referred to brittle characteristic of epoxy resin. It can be observed that the addition of MWCNTs into polymer matrix

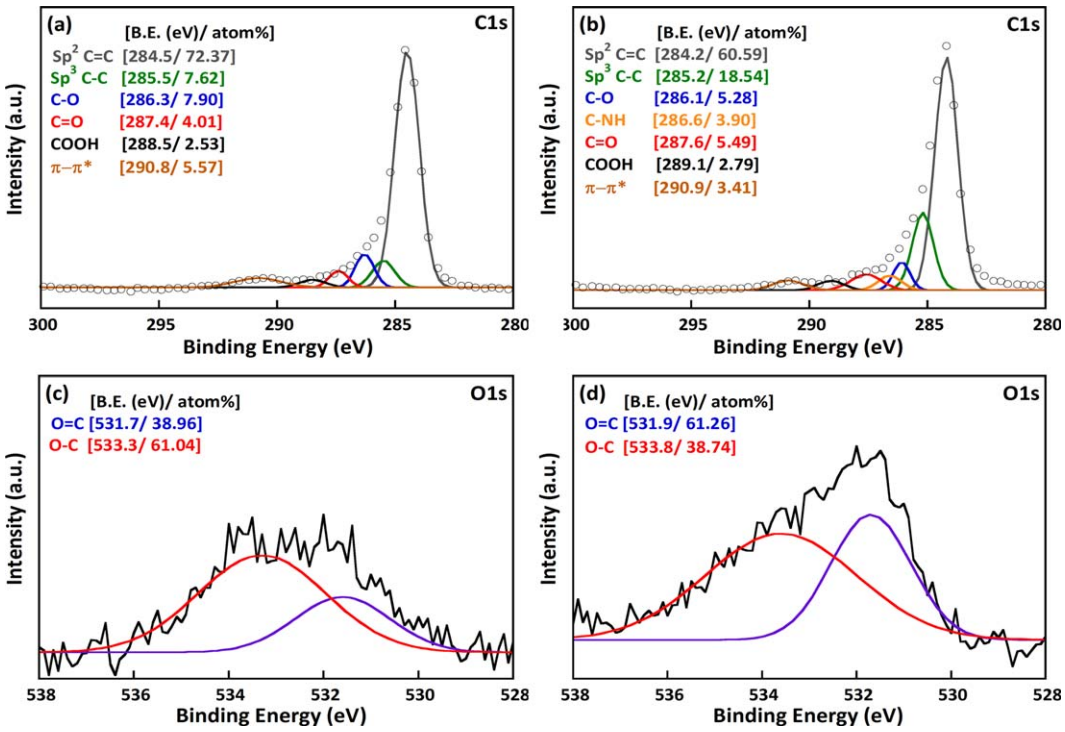

Figure 4. High-resolution XPS spectra for C1s and O1s regions of (a, c) U-MWCNTs and (b, d) DAB-MWCNTs. [Color figure can be viewed in the online issue, which is available at wileyonlinelibrary.com.]

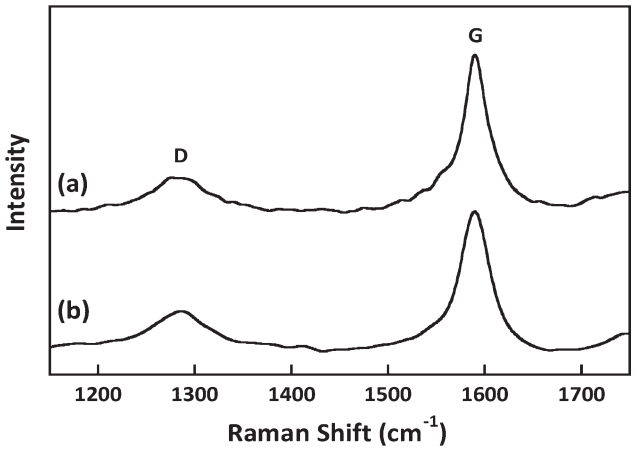

Figure 5. FT-Raman spectra of (a) U-MWCNTs and (b) DAB-MWCNTs.

afforded greater roughness of fracture surface, which related to the toughness improvement of composites. Nonetheless, U-MWCNTs exhibit poor dispersion within polymer matrix in which large bundles of U-MWCNTs can be observed when U-MWCNT loading increase, as seen in Figure 7(c). It is due to their high surface area and high van der Waals force between the nanotubes. After the functionalization, DAB-MWCNTs were dispersed more homogeneously in polymer matrix. The small white dots, representing the broken ends of embedded MWCNTs, were mainly observed in the composite as shown in Figure 7(d). This phenomenon might be due to enhanced dispersibility and interfacial interaction caused by diaminobenzoyl functional groups established on the surface of DAB-MWCNTs.

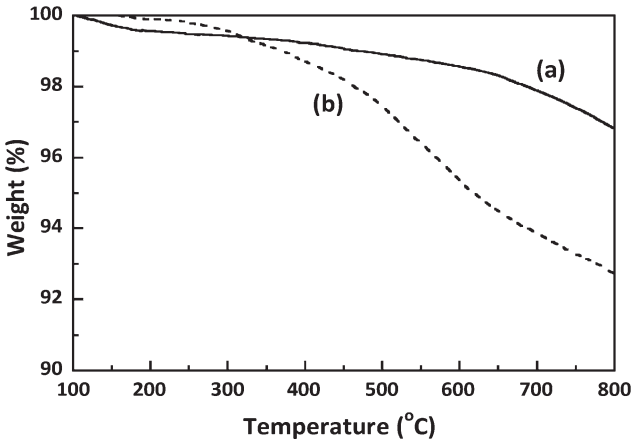

Figure 6. TGA curves of (a) U-MWCNTs and (b) DAB-MWCNTs in N_2 atmosphere.

Moreover, the dispersion of hybrid fillers containing MWCNTs and Si_3N_4 particles in the polymer matrix was evaluated as shown in Figure 7(e,f). The fracture surface of composite reinforced with U-MWCNTs and Si_3N_4 fillers is quite smooth. It might be due to the heterogeneous distribution of fillers in epoxy matrix and weak interfacial interaction between fillers and polymer matrix. However, the addition of hybrid filler based on DAB-MWCNTs into polymer matrix provided more roughness of fracture surface. It is because amino groups of DAB moieties on their surface improved the dispersion of fillers in the matrix and enhanced interfacial interaction between fillers and the polymer matrix.

Dynamic Mechanical Properties of Epoxy Composites

In this section, the dynamic mechanical properties of epoxy composites reinforced with U-MWCNTs and DAB-MWCNTs at low concentration are discussed. The plots of storage modulus (E') and loss modulus (E'') as a function of temperature for epoxy composites filled with various loading of U-MWCNTs and DAB-MWCNTs are illustrated in Figures 8 and 9, respectively. Comparing with neat epoxy resin, all composites exhibit higher E', indicating the increase of stiffness. As can be seen in Figure 8(a), the storage moduli at room temperature of U-MWCNT/epoxy composites increased with increasing filler concentration because of their high aspect ratio and excellent mechanical properties. However, the decrease of E' was found at high loading of U-MWCNTs. It is explained by considering the fact that U-MWCNTs were easily entangled and formed large agglomerates in epoxy matrix because of high surface area and high intrinsic van der Waals force between the nanotubes. Evidently, E′ of DAB-MWCNT/epoxy composites linearly increased as a function of volume fraction as shown in Figure 9(a) and was higher than that of U-MWCNTs at the same filler loading. It can be attributed to well homogeneous dispersion of DAB-MWCNTs in the polymer matrix after the functionalization. It is mainly because the presence of amino groups in DAB structure and oxygen-containing groups on their surface led to the decrease of van der Waals force among the nanotubes. Another possible reason to explain this phenomenon is better interfacial interaction between the nanotube and polymer matrix. The existence of amino groups and small amount of oxygen containing groups on MWCNTs could provide fairly strong interaction with epoxy resin, corresponding to effective load and heat transfer from MWCNTs through epoxy matrix. According to the DMA analysis, the cross-link density (λ) can be estimated from the plateau of E' in the rubbery state as given by[28,29]

$$\lambda = \frac{E'}{3RT} \quad (1)$$

where E' is the storage modulus at $T_g + 50°C$; R is the gas constant; and T is the absolute temperature at $T_g + 50°C$. The

Table II. FT-Raman Results of Unmodified and Functionalized MWCNTs

	Intensity			
Material	D band	G band	FWHM[a]	I_D/I_G
U-MWCNT	0.204	0.855	32.25	0.449
DAB-MWCNT	0.236	0.896	36.93	0.455

Applied Polymer SCIENCE

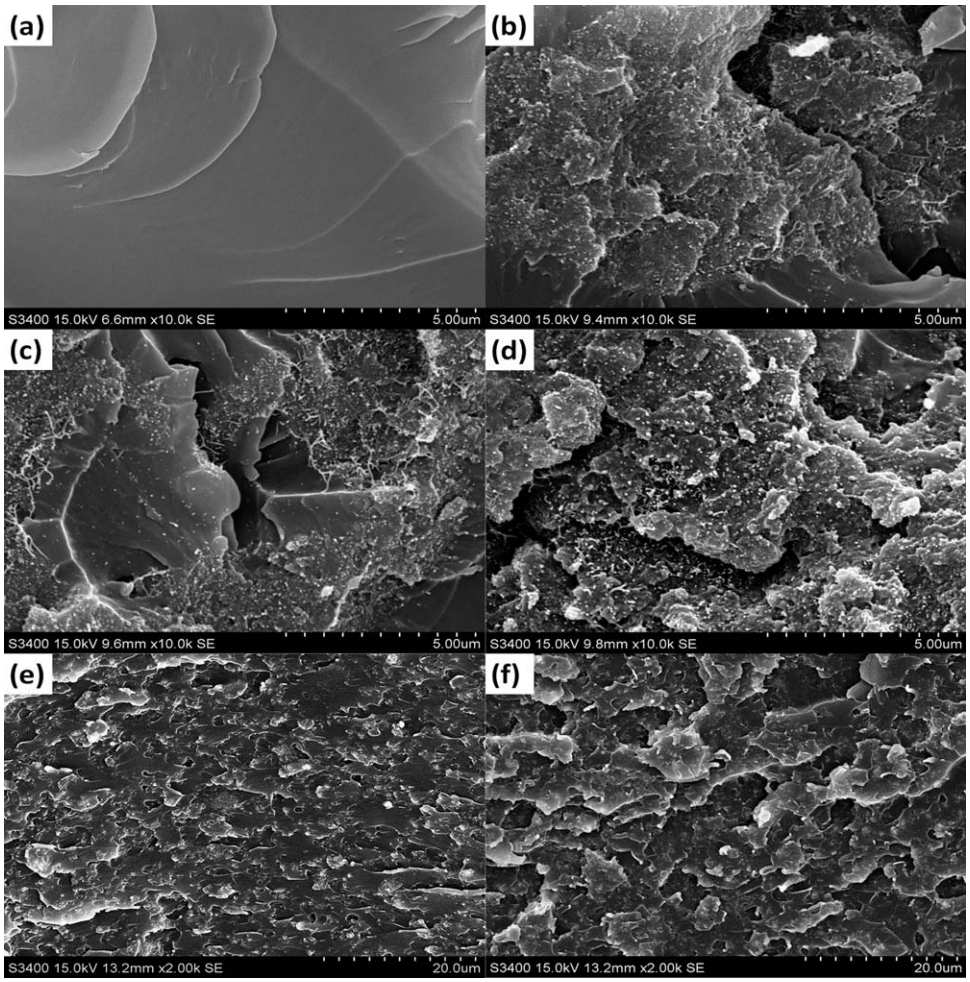

Figure 7. Fracture surfaces of (a) neat epoxy and composites filled with (b) U-MWCNT 0.5 vol %, (c) U-MWCNT 1.0 vol %, (d) DAB-MWCNT 1.0 vol %, (e) U-MWCNT 1.0 vol %-Si_3N_4 7.5 vol %, and (f) DAB-MWCNT 1.0 vol %-Si_3N_4 7.5 vol %.

calculated crosslink density of epoxy composites is shown in Figure 10(a). It is well known that the epoxide group can be attacked by amine or carboxyl acid and then form the crosslinking structure of epoxy resin via nucleophilic addition reaction. With the addition of U-MWCNTs, the crosslink density of composites slightly increased. It is believed that small amounts of oxygen-containing groups embedded on the MWCNT surface probably reacted with the oxirane rings in epoxy monomer, providing more crosslink degree. In case of DAB-MWCNT/epoxy composites, the diamino functional groups of DAB introduced onto the surface of MWCNTs could react with epoxy monomers and formed additional crosslink networks in composites. Thus, the crosslink density of DAB-MWCNT/epoxy composites linearly increased as a function of volume fraction and was higher than that of U-MWCNTs as well.

Moreover, the measurement of the glass transition temperature (T_g) of composite which is one of the most important applications based on DMA analysis was carried out. Conventionally, the T_g can be observed at the temperature where the E'' reaches the maximum value. Figures 8(b) and 9(b) illustrate the loss moduli of epoxy composites reinforced with U-MWCNTs and DAB-MWCNTs as a function of temperature, respectively. The E'' peaks obviously shifted to higher temperature at very low loading of MWCNTs, indicating the T_g enhancement. This phenomenon is attributed to the existence of randomly dispersed U-MWCNTs in epoxy matrix restricted the mobility of polymer chains. It is known that the T_g of polymer composite substantially related to the mobility of polymer segments or the free volume fraction in polymer. Nonetheless, the T_g of composites slightly decreased with further increase of U-MWCNT contents. It can be definitely considered that large bundles of U-MWCNTs dispersed heterogeneously in polymer matrix possibly interrupted the formation of crosslink networks in the composites. This behavior is consistent with the insignificant change in the crosslink density of U-MWCNT/epoxy composites when the filler loading was higher than 0.5 vol %. In contrast, the T_g of composites noticeably increased with the incorporation of DAB-MWCNTs because of the good dispersion and greatly improved interfacial interaction after the functionalization as discussed previously. Figure 10(b) demonstrates the plot of T_g versus filler volume fraction of composites. Besides, the increase of crosslink density in composites referred to the decrease of free volume fraction could restrict the polymer mobility, leading to high T_g.[30–32]

Additionally, the storage moduli and loss moduli of composites containing hybrid fillers are illustrated in Figure 11. It can be

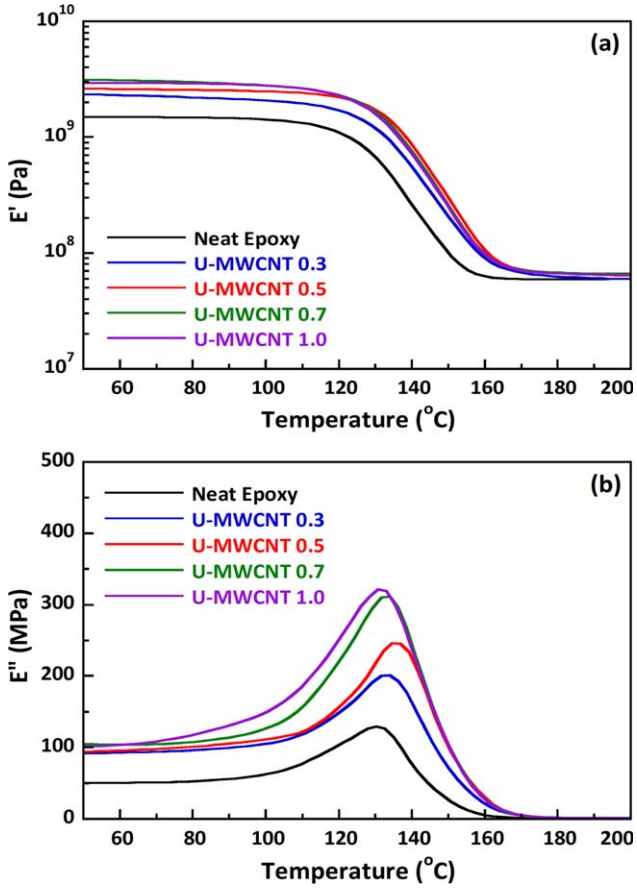

Figure 8. Dynamic mechanical properties of epoxy composites reinforced with U-MWCNTs: (a) storage modulus and (b) loss modulus. [Color figure can be viewed in the online issue, which is available at wileyonlinelibrary.com.]

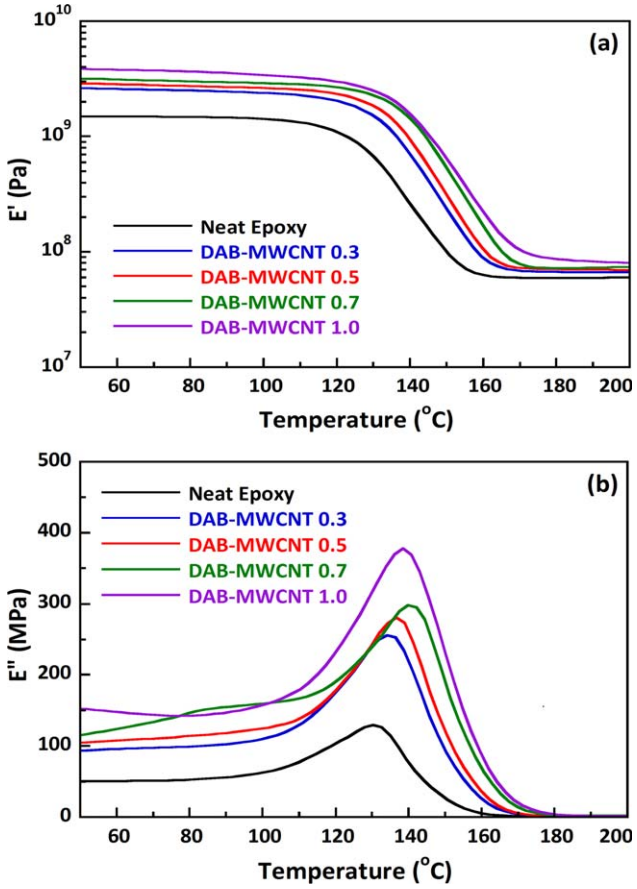

Figure 9. Dynamic mechanical properties of epoxy composites reinforced with DAB-MWCNTs: (a) storage modulus and (b) loss modulus. [Color figure can be viewed in the online issue, which is available at wileyonlinelibrary.com.]

seen that E' of epoxy composites filled with hybrid filler were higher than that with single filler. The E' increased with increasing of Si_3N_4 content. The effective reinforcement of submicron-sized Si_3N_4 particles may be attributed to their rigidity and intrinsic high modulus. From the results of E'' peak, it reveals that the addition of Si_3N_4 particles into U-MWCNT based polymer composites slightly enhanced their T_g. It is possibly because the increase of filler concentration could reduce the free volume fraction. Considering the hybrid filler system containing 1.0 vol % DAB-MWCNTs and 7.5 vol % Si_3N_4, the composite exhibits high E' and high T_g. It is believed that these behaviors are attributed to the presence of amino groups that promoted good dispersion of fillers and better interfacial interaction, possibly hindering polymer chain mobility and reducing free volume fraction in the composite.[31] However, the addition of submicron-sized Si_3N_4 fairly obstructed the formation of crosslink structures in composites, decreasing the crosslink density. The T_g and crosslink density of epoxy composites added with hybrid fillers are determined and shown in Table III.

Thermal Properties of Epoxy Composites

The linear thermal expansion as a function of temperature was investigated using TMA. Generally, the linear thermal expansion of polymer composite gradually increased in a glassy state due to

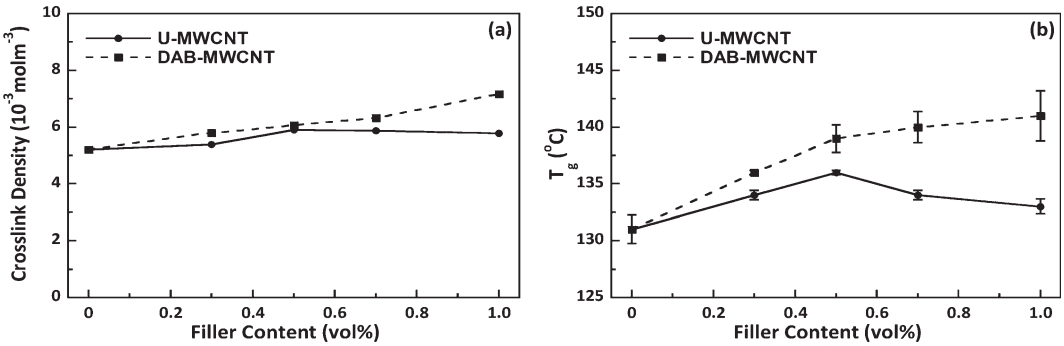

Figure 10. (a) The crosslink density and (b) the glass transition temperature of epoxy composites.

Applied Polymer SCIENCE

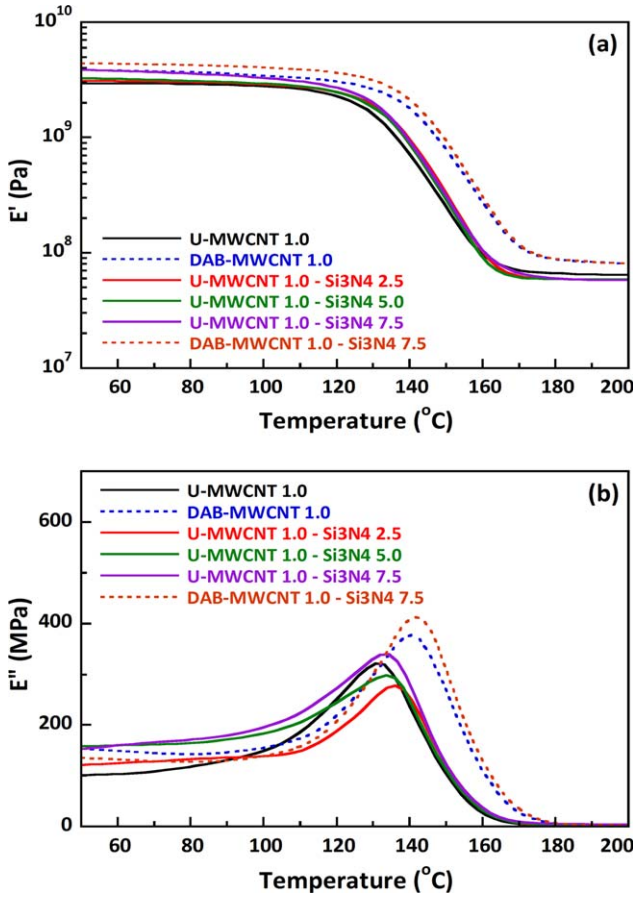

Figure 11. Dynamic mechanical properties of epoxy composites reinforced with various hybrid fillers: (a) storage modulus and (b) loss modulus. [Color figure can be viewed in the online issue, which is available at wileyonlinelibrary.com.]

rigidity of crosslink materials. Then, it sharply increased in the rubbery state because polymer chains were more flexible and dilated at temperature higher than T_g. The CTE was determined from a slope of a plot between linear thermal expansion and temperature, which was commonly reported in the glassy state. As illustrated in Figure 12(a), the CTE decreased as the volume fraction of fillers increased, resulting in decrease of free volume fraction as mentioned in our previous work.[31,32] Especially DAB-MWCNT/epoxy composites, diamino groups on the DAB-MWCNT surface probably formed the chemical bonding with epoxy resin, increasing the crosslink density and reducing the free volume fraction. As shown in Figure 12(b), the addition of hybrid fillers as MWCNTs and Si_3N_4 particles into polymer matrix provided rather low CTE because of low intrinsic CTE of fillers. Especially, the CTE of composite remarkably reduced by the incorporation of hybrid fillers based on DAB-MWCNTs into epoxy matrix. It is possibly due to optimal packing density of DAB-MWCNTs and Si_3N_4 particles, caused by amino functional groups of DAB-MWCNTs that effectively formed filler-filler interaction. It has a positive effect on thermal stability of composites, thus the CTE of epoxy composites remarkably decreased.

Thermal Conductivity of Epoxy Composites

To elucidate the effect of MWCNT concentration and the functionalization on the thermal conductivity of composite, the values of thermal conductivity were calculated from the equation

$$K = \alpha \rho C_p \quad (2)$$

where K, α, ρ, and C_p are the thermal conductivity of composites, thermal diffusivity, density, and heat capacity, respectively. The density of MWCNT/epoxy composites was measured by water displacement, which can be given by

$$\rho = \frac{W_{dry}}{W_{dry} - W_{Wet}} \rho_{water}(T) \quad (3)$$

and the theoretical density of composites was also calculated by using a following equation

$$\rho = \rho_m \left(1 - \sum_{i-1}^{n} v_i\right) + \sum_{i-1}^{n} \rho_i v_i \quad (4)$$

where ρ, ρ_m, and ρ_i are the density of composite, polymer matrix, and filler, respectively; and V_i is the volume fraction of filler. The comparison between the measured and theoretical density is illustrated in Figure 13(a). The measured density is very close to the theoretical density. Figure 13(b,c) shows the temperature dependence of thermal diffusivity of composites incorporated with U-MWCNTs and DAB-MWCNTs, respectively. For all samples, the thermal diffusivity gradually decreased as the temperature increased. However, the thermal diffusivity of composites remarkably increased by adding small amounts of fillers. Clearly, the thermal diffusivity of DAB-MWCNT/epoxy composites is higher than that obtained from U-MWCNT/epoxy composites. It is possibly due to good interfacial interaction between DAB-MWCNT and polymer matrix caused by the functionalization. Figure 13(d) shows the thermal conductivity of epoxy composites at 50°C. At very low concentration, U-MWCNTs were randomly dispersed in polymer matrix and provided heat conductive pathways in the polymer matrix. Thus, thermal conductivity of composites was higher than that of neat epoxy. With further increase of U-MWCNT loading, thermal conductivity scarcely increased. It is attributed to their high surface area, high aspect ratio, and high van der Waals force between the nanotubes, causing the heterogeneous dispersion of U-MWCNTs at high volume fraction in

Table III. Properties of Epoxy Composites Filled with Various Hybrid Fillers

Material	T_g (°C)	λ (10^{-3}mol m^{-3})	ρ (g cm^{-3})	α (mm^2 s^{-1})	K (W m^{-1} K^{-1})
U-MWCNT 1.0-Si_3N_4 2.5	136	5.132	1.2584	0.145	0.255
U-MWCNT 1.0-Si_3N_4 5.0	136	5.095	1.3202	0.166	0.304
U-MWCNT 1.0-Si_3N_4 7.5	134	5.094	1.3865	0.170	0.324
DAB-MWCNT 1.0-Si_3N_4 7.5	142	6.898	1.3818	0.175	0.367

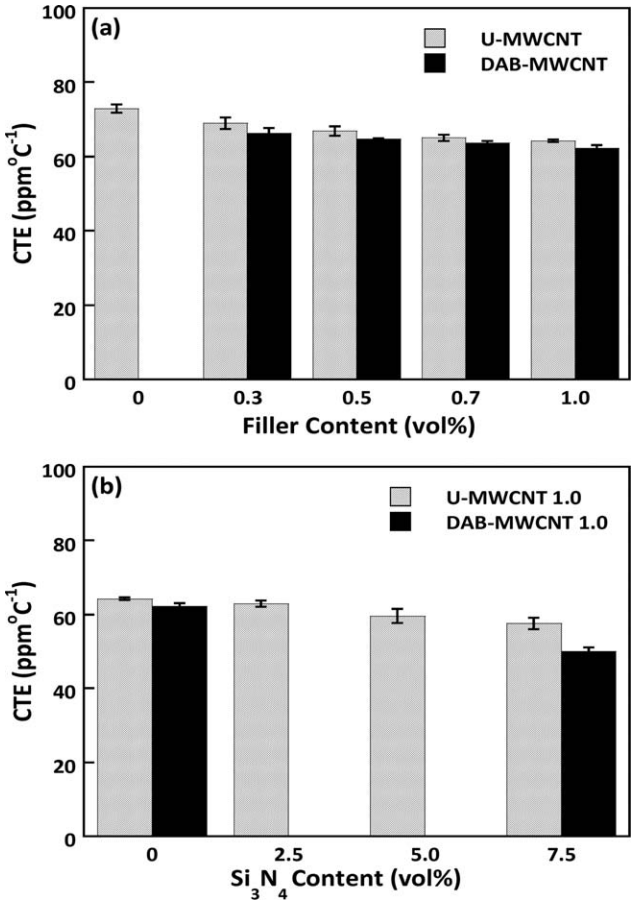

Figure 12. CTE of epoxy composites filled with (a) single filler systems and (b) hybrid filler systems.

polymer matrix as seen in SEM images. This behavior hindered the potential of U-MWCNTs. After the functionalization with DAB, the dispersion of DAB-MWCNTs within epoxy resin was greatly improved. The DAB moieties on their surface provided better interfacial interaction between DAB-MWCNT and polymer matrix, reducing the interfacial thermal resistance. The effective heat conductive pathways were provided in the composite. Therefore, the thermal conductivity of epoxy composites increased as a function of DAB-MWCNT concentration. In addition, thermal conductivity of epoxy filled with DAB-MWCNTs was higher than that of U-MWCNTs at the same filler loading.

To investigate the effect of the addition of thermally conductive filler on the thermal conductivity of polymer composites, various theoretical and empirical models have been developed.[1633–35] The most common equations based on Maxwell-Eucken's and Lewis-Nielsen's models were used in this work to predict the thermal conductivity of epoxy composites.

The Maxwell-Eucken's model can be use to predict the thermal conductivity of composites by

$$K=K_m\frac{[K_f+2K_m+2V_f(K_f-K_m)]}{[K_f+2K_m-V_f(K_f-K_m)]} \quad (5)$$

where K, K_m, and K_f are the thermal conductivity of composites, polymer matrix and filler, respectively; V_f is the volume fraction of filler. It was clearly seen that the experimental data were higher than those predicted values, which is due to the assumption of this model, which indicates that the fillers are spherical particles without mutual interaction dispersed randomly in the polymer matrix.[36] While, MWCNTs used in this work have extremely high aspect ratio and the mutual interaction with each other. Therefore, MWCNTs could provide more heat conductive networks in the composite, resulting in the enhancement of thermal conductivity. It is, especially true for, DAB-MWCNTs because the DAB functional groups on their surface could achieve good dispersion and interaction between the polymer matrix and filler as mentioned above.

The Lewis-Nielsen's model was further applied to evaluate the thermal conductivity of composites by taking the geometry and the maximum volume fraction of filler into the consideration.[37] It can be explained by

$$K=K_m\frac{1+ABV_f}{1-B\,\Psi\,V_f} \quad (6)$$

where

$$A=K_E-1, \quad (7)$$

$$B=\frac{K_f/K_m-1}{K_f/K_m+A'} \quad (8)$$

$$\Psi=1+\left(\frac{1-V_m}{V_{m^2}}\right)V_f, \quad (9)$$

where K_E is an Einstein constant related to the shape and orientation of the filler; B is a factor depending on the thermal conductivity of each component; V_m is the maximum packing fraction of filler; and ψ is a parameter related to the volume fraction of filler. Generally, the values of A and V_m are constant for each type of filler. For instance, $A = 8.38$ and $V_m = 0.52$ are often used for the polymer composites based on the short fibers with aspect ratio less than 15 randomly dispersed in 3D direction. As shown in Figure 13(d), the experimental values of thermal conductivity of epoxy composites incorporated with U-MWCNTs and DAB-MWCNTs was compared with that obtained from this model. It was found that the experimental values did not fit well with the predicted values. The thermal conductivity based on this model was close to the experimental values rather than those calculated from Maxwell-Eucken's model. It is because this model is the most versatile for the particulate/short fiber composites, whereas MWCNTs are much stronger and have larger high aspect ratio than the conventional fibers. Beside, the value of A, which strongly affects the prediction, is not suitable for MWCNT/polymer composites.

As mentioned above, the measured thermal conductivity of MWCNT/epoxy composites was fairly higher than those predicted from the conventional models. Consequently, the effective medium approaches (EMA) have been proposed to evaluate the effective thermal conductivity of polymer composites.[38] The Maxwell-Garnett (MG) typed EMA has been found suitable for predicting the thermal conductivity of polymer composites filled with low concentration of MWCNTs.[39] The MG-EMA was built on the basis of a random orientation of MWCNTs and high aspect ratio ($P > 1000$).[40]

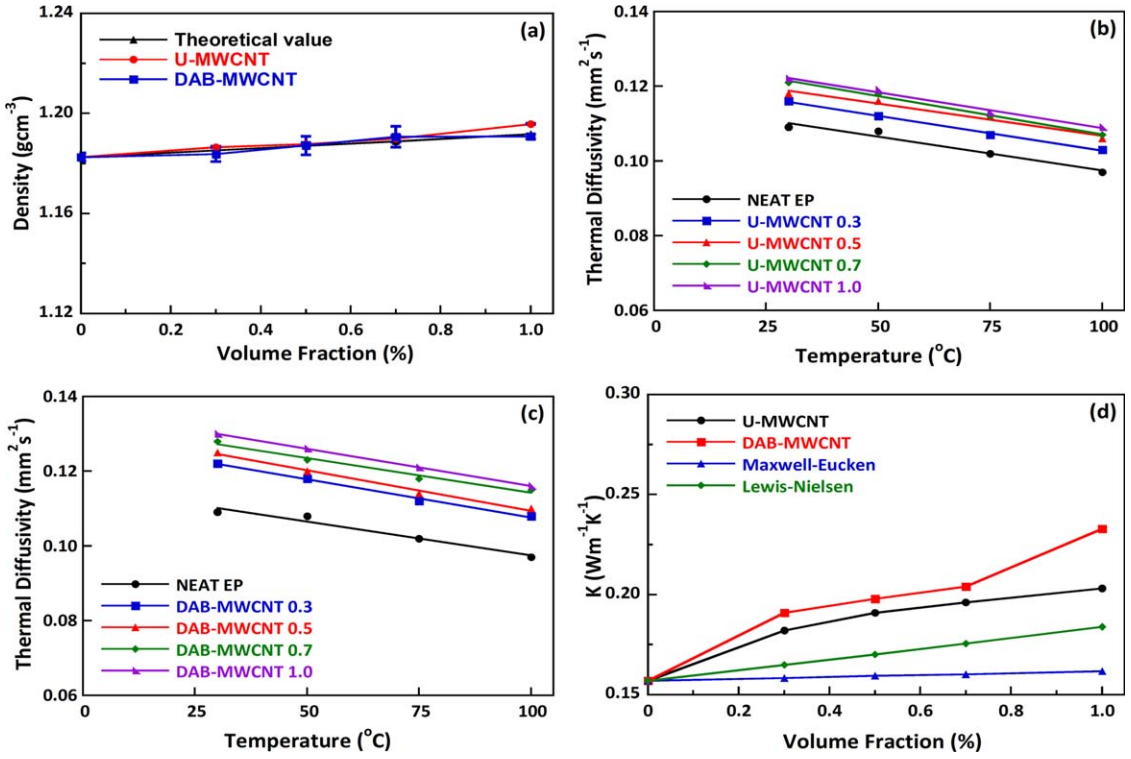

Figure 13. Properties of epoxy composites: (a) density, (b) thermal diffusivity of U-MWCNT/epoxy composites, (c) thermal diffusivity of DAB-MWCNT/epoxy composites, and (d) thermal conductivity. [Color figure can be viewed in the online issue, which is available at wileyonlinelibrary.com.]

The MG-EMA equation can be expressed as

$$\frac{K_e}{K_m}=\frac{3+2V_f[\beta_x(1-L_x)+\beta_z(1-L_z)]}{3-V_f(2\beta_x L_x+\beta_z L_z)}, \quad (10)$$

where K_e is the effective thermal conductivity of composite; K_m and K_f are the thermal conductivity of polymer matrix and filler, respectively; and V_f is the volume fraction of filler. β_x and β_z are defined as

$$\beta_x=\frac{K_x-K_m}{K_m+L_x(K_f-K_m)}, \quad (11)$$

$$\beta_z=\frac{K_z-K_m}{K_m+L_z(K_f-K_m)}, \quad (12)$$

where K_x and K_z are the thermal conductivity of MWCNTs along transverse and longitudinal axes, respectively. L_x and L_z are the geometrical factors depending on the aspect ratio (P) of MWCNTs, given by

$$L_x=\frac{p^2}{2(p^2-1)}-\frac{p}{2(p^2-1)^{3/2}}\cosh^{-1}p, \quad (13)$$

$$L_z=1-2L_x, \quad (14)$$

The high aspect ratio ($P > 100$) of MWCNTs gives $L_x = 0.5$ and $L_z = 0$. If K_x and K_z of MWCNTs are much larger than K_m, then eq. (10) can be simplified as[39]

$$\frac{K_e}{K_m}=\frac{3+V_fK_f/K_m}{3-2V_f}. \quad (15)$$

Figure 14(a) shows the effective thermal conductivity (K_e) of composite as a function of MWCNT loading. As seen, the simplified equation predicted much higher thermal conductivity

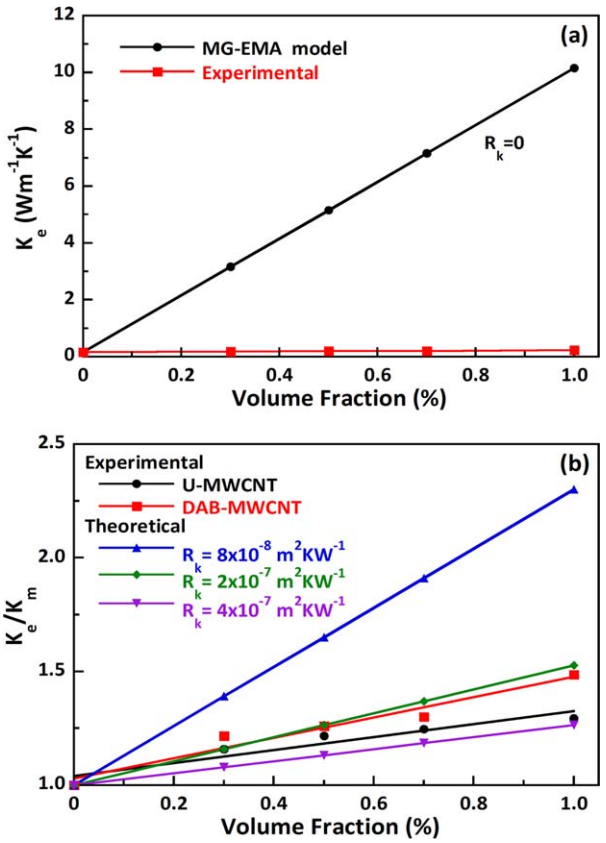

Figure 14. Effective thermal conductivity of epoxy composites incorporated with (a) single filler systems and (b) hybrid filler systems at 50°C. [Color figure can be viewed in the online issue, which is available at wileyonlinelibrary.com.]

than the experimental values. The deviation between the theoretical and experimental values is possibly due to the interfacial thermal resistance (R_k) between the nanotube and the polymer matrix. Therefore, the K_e in eq. (15) was developed by considering the perfect interface without any interfacial thermal resistance ($R_k = 0$). The modified MG-EMA model was developed by taking the interfacial thermal resistance into the consideration in term of Kapitza radius (a_k), which can be described as a following expression[41,42]

$$\frac{K_e}{K_m} = 1 + \frac{V_f p}{3} \frac{K_f/K_m}{p + \frac{2a_k}{d}\frac{K_f}{K_m}} \quad (16)$$

where

$$a_k = R_k K_m \quad (17)$$

Figure 14(b) shows the predicted K_e/K_m ratio with various R_k values. The enhancement of thermal conductivity was noticeably observed with low R_k. The measured values for U-MWCNT/epoxy composites were close to the predicted values according to eq. (16) with $R_k = 4 \times 10^{-7}$ m^2 KW^{-1}, whereas the experimental data for DAB-MWCNT/epoxy composites fit quite well with the theoretical values when R_k is about 2×10^{-7} m^2 KW^{-1}. These results indicated that the interfacial thermal resistance slightly decreased after the functionalization. The amino groups in the DAB structure established on the surface of MWCNTs could provide chemical bonding between DAB-MWCNT and epoxy resin, resulting in the decrease of interfacial thermal resistance. Therefore, the thermal conductivity of DAB-MWCNT/epoxy composites greatly enhanced.

To obtain higher thermal conductivity of composites, MWCNTs were partially replaced with submicron-sized fillers. The effects of hybrid filler systems on the thermal conductivity were investigated and summarized in Table III. The 1.0 vol % U-MWCNTs filled epoxy composites were incorporated with various contents of Si_3N_4 particles. It was found that thermal conductivity increased with increasing Si_3N_4 content. The addition of submicron-sized fillers in the composites promoted more heat conductive pathways and high packing density, enhancing the heat dissipation of materials. In case of epoxy resin filled with 1.0 vol % DAB-MWCNTs and 7.5 vol % Si_3N_4, the heat conductive networks were effectively formed with optimal packing density, thereby increasing thermal conductivity more than 134% compared with that of neat epoxy. This result confirms that the hybrid fillers can be used as effective filler to improve the thermal conductivity of composites.

CONCLUSIONS

DAB was successfully introduced onto the surface of MWCNTs with less structural damage. The amino functional groups on the DAB-MWCNT surface enhanced filler dispersion in epoxy composite. The composites reinforced with DAB-MWCNTs remarkably exhibit high E', high T_g and low CTE rather than those of U-MWCNTs at the same filler content. Amino groups of diaminobenzoyl compound promoted strong interfacial interaction between DAB-MWCNT and polymer matrix that can reduce the interfacial thermal resistance, resulting in an increase of thermal conductivity. The modified MG-EMA model by considering the interfacial thermal resistance is appropriate for predicting the thermal conductivity of epoxy composites filled with low concentration of MWCNTs. The properties of epoxy composites reinforced with hybrid filler systems were also studied. According to the results, the hybrid filler systems were effective filler to enhance dynamic mechanical properties and thermal properties of composites. Especially, the hybrid filler containing 1.0 vol % DAB-MWCNTs and 7.5 vol % Si_3N_4 promoted effective heat conductive pathways and optimal packing density in polymer matrix, thereby achieving 134% higher thermal conductivity than that of neat epoxy resin.

ACKNOWLEDGMENTS

The authors would like to thank Advance Material Cluster, Chulalongkorn University and Mektec Manufacturing Corporation (Thailand) Ltd. for financial and material supports. The authors thank the Center of Excellence on Catalysis and Catalytic Reaction Engineering, Department of Chemical Engineering, Faculty of Engineering, Chulalongkorn University for XPS analysis. We would like to acknowledge Prof. Piyasan Praserthdam, project's PI for valuable discussion and suggestion.

REFERENCES

1. Zhou, T.; Wang, X.; Mingyuan, G. U.; Liu, X. *Polymer* **2008**, *49*, 4666.
2. Gu, J. W.; Zhang, Q. Y.; Dang, J.; Xie, C. *Polym. Adv. Technol.* **2012**, *23*, 1025.
3. Zhu, B. L.; Ma, J.; Wu, J.; Yung, K. C.; Xie, C. S. *J. Appl. Polym. Sci.* **2010**, *118*, 2754.
4. Li, S. S.; Qi, S. H.; Liu, N. L.; Cao, P. *Thermochim. Acta* **2011**, *523*, 111.
5. Yu, H.; Li, L. L.; Kido, T.; Xi, G. N.; Xu, G. C.; Guo, F. *J. Appl. Polym. Sci.* **2012**, *124*, 669.
6. Yang, K.; Gu, M.; Guo, Y.; Pan, X.; Mu, G. *Carbon* **2009**, *47*, 1723.
7. Theodore, M.; Hosur, M.; Thomas, J.; Jeelani, S. *Mater. Sci. Eng. A* **2011**, *528*, 1192.
8. Han, S. W.; Oh, S. J.; Tan, L. S.; Baek, J. B. *Carbon* **2008**, *46*, 1841.
9. Lee, H.-J.; Han, S.-W.; Kwon, Y.-D.; Tan, L.-S.; Baek, J.-B. *Carbon* **2008**, *46*, 1850.
10. Yang, S.-Y.; Ma, C.-C. M.; Teng, C.-C.; Huang, Y.-W.; Liao, S.-H.; Huang, Y.-L.; Tien, H.-W.; Lee, T.-M.; Chiou, K.-C. *Carbon* **2010**, *48*, 592.
11. Teng, C.-C.; Ma, C.-C. M.; Chiou, K.-C.; Lee, T.-M.; Shih, Y.-F. *Mater. Chem. Phys.* **2011**, *126*, 722.
12. Teng, C.-C.; Ma, C.-C. M.; Chiou, K.-C.; Lee, T.-M. *Compos. Part B Eng.* **2012**, *43*, 265.
13. Yang, K.; Gu, M. *Compos. Part A: Appl. Sci. Manuf.* **2010**, *41*, 215.
14. Zhou, T.; Wang, X.; Liu, X.; Xiong, D. *Carbon* **2010**, *48*, 1171.

15. He, H.; Fu, R.; Shen, Y.; Han, Y. C.; Song, X. F. *Compos. Sci. Technol.* **2007**, *67*, 2493.
16. An, Q. L.; Qi, S. H.; Zhou, W. Y. *Polym. Compos.* **2009**, *30*, 866.
17. Zhou, W.; Wang, C.; Ai, T.; Wu, K.; Zhao, F.; Gu, H. *Compos. Part A: Appl. Sci. Manuf.* **2009**, *40*, 830.
18. Shi, Z.; Fu, R.; Agathopoulos, S.; Gu, X.; Zhao, W. *Mater. Des.* **2012**, *34*, 820.
19. Geng, Y.; Liu, M. Y.; Li, J.; Shi, X. M.; Kim, J. K. *Compos. Part A: Appl. Sci. Manuf.* **2008**, *39*, 1876.
20. Koysuren, O.; Karaman, M.; Ozyurt, D. *J. App. Polym. Sci.* **2013**, *127*, 4557.
21. Cividanes, L. S.; Brunelli, D. D.; Antunes, E. F.; Corat, E. J.; Sakane, K. K.; Thim, G. P. *J. App. Polym. Sci.* **2013**, *127*, 544.
22. Jeon, I.-Y.; Kang, S.-W.; Tan, L.-S.; Baek, J.-B. *J. Polym. Sci. Part A: Polym. Chem.* **2010**, *48*, 3103.
23. Chen, W.; Qian, X.-M.; He, X.-Q.; Liu, Z.-Y.; Liu, J.-P. *J. App. Polym. Sci.* **2012**, *123*, 1983.
24. Kundu, S.; Wang, Y.; Xia, W.; Muhler, M. *J. Phys. Chem. C* **2008**, *112*, 16869.
25. Okpalugo, T. I. T.; Papakonstantinou, P.; Murphy, H.; McLaughlin, J.; Brown, N. M. D. *Carbon* **2005**, *43*, 153.
26. Rong, H.; Han, K.; Li, S.; Tian, Y.; *Muhuoyu J. Appl. Polym. Sci.* **2013**, *127*, 2033.
27. Liu, H.; Wang, X.; Fang, P.; Wang, S.; Qi, X.; Pan, C.; Xie, G.; Liew, K. M. *Carbon* **2010**, *48*, 721.
28. Liu, W. S.; Wang, Z. G.; Chen, Z.; Li, J. F.; Zhao, L. N. *Polym. Adv. Technol.* **2012**, *23*, 367–374.
29. Miyagawa, H.; Misra, M.; Drzal, L. T.; Mohanty, A. K. *Polym. Eng. Sci.* **2005**, *45*, 487.
30. Montazeri, A.; Pourshamsian, K.; Riazian, M. *Mater. Des.* **2012**, *36*, 408.
31. Pongsa, U.; Samthong, C.; Somwangthanaroj, A. *Polym. Eng. Sci.,* to appear. DOI: 10.1002/pen.23472.
32. Samthong, C.; Laine, R. M.; Somwangthanaroj, A. *J. App. Polym. Sci.,* to appear. DOI: 10.1002/app.38575.
33. Shen, M.-x.; Cui, Y.-x.; He, J.; Zhang, Y.-m. *Int. J. Min. Met. Mater.* **2011**, *18*, 623.
34. Weber, E. H.; Clingerman, M. L.; King, J. A. *J. App. Polym. Sci.* **2003**, *88*, 123.
35. Li, S. S.; Qi, S. H.; Liu, N. L.; Cao, P.; Zhang, Y. *J. App. Polym. Sci.* **2012**, *124*, 4403.
36. Tu, H.; Ye, L. *J. Appl. Polym. Sci.* **2010**, *116*, 2336.
37. Gaxiola, D. L.; Keith, J. M.; King, J. A.; Johnson, B. A. *J. Appl. Polym. Sci.* **2009**, *114*, 3261.
38. Clancy, T. C.; Frankland, S. J. V.; Hinkley, J. A.; Gates, T. S. *Int. J. Therm. Sci.* **2010**, *49*, 1555.
39. Nan, C. W.; Shi, Z.; Lin, Y. *Chem. Phys. Lett.* **2003**, *375*, 666.
40. Nan, C.-W.; Liu, G.; Lin, Y.; Li, M. *Appl. Phys. Lett.* **2004**, *85*, 3549.
41. Im, H.; Kim, J. *Carbon* **2012**, *50*, 5429.
42. Clancy, T. C.; Gates, T. S. *Polymer* **2006**, *47*, 5990.